Research Article | Vol. 29, No. 18 / 30 Aug 2021 / Optics Express 28452

Optics EXPRESS

Ultra-dense perfect optical orbital angular momentum multiplexed holography

GUOXUAN ZHU,[1,2] ZHIYONG BAI,[1,2,*] JIAYAN CHEN,[1] CHUROU HUANG,[1] LUPING WU,[1] CAILING FU,[1,2] AND YIPING WANG[1,2]

[1] *Key Laboratory of Optoelectronic Devices and Systems of Ministry of Education/Guangdong Province, College of Physics and Optoelectronic Engineering, Shenzhen University, Shenzhen 518060, China*

[2] *Shenzhen Key Laboratory of Photonics Devices and Sensing Systems for Internet of Things, Guangdong and Hong Kong Joint Research Centre for Optical Fiber Sensors, Shenzhen University, Shenzhen 518060, China*

[*] *baizhiyong@szu.edu.cn*

Abstract: Optical orbital angular momentum (OAM) has been recently implemented in holography technologies as an independent degree of freedom for boosting information capacity. However, the holography capacity and fidelity suffer from the limited space-bandwidth product (SBP) and the channel crosstalk, albeit the OAM mode set exploited as multiplexing channels is theoretically unbounded. Here, we propose the ultra-dense perfect OAM holography, in which the OAM modes are discriminated both radially and angularly. As such, the perfect OAM mode set constructs the two-dimensional spatial division multiplexed holography (conventional OAM holography is 1D). The extending degree of freedom enhances the holography capacity and fidelity. We have demonstrated an ultra-fine fractional OAM holography with the topological charge resolution of 0.01. A 20-digit OAM-encoded holography encryption has also been exhibited. It harnesses only five angular OAM topological charges ranging from -16 to +16. The SBP efficiency is about 20 times larger than the conventional phase-only OAM holography. This work paves the way to compact, high-security and high-capacity holography.

1. Introduction

Optical holography technology reconstructs the beam field with computer-generated holograms (CGHs) and has achieved great success in diverse applications, including artificial intelligence [1,2], optical tweezers [3,4], 3D printing [5], optical computing [6] and information storage [7,8]. The conventional holography uses polarization, wavelength and incident angle as the independent multiplexing channel sets [9–11], which are married with limited spatial channel availability and substantial crosstalk. Recently, optical orbital angular momentum (OAM) has been exploited as an additional information carrier in holography, hence boosting the system capacity and security [12,13]. The OAM set, characterized by angular vortex phase $\exp(il\varphi)$, where l is the topological charge (TC), can theoretically provide unlimited distinct mode channels for multiplexing [14–16]. Abundant multiplexing resources can lift the capacity of hologram and suppress the channel crosstalk [17,18]. The verification of OAM capacity has been witnessed in various fields besides holography, such as information storage [19], quantum key distribution [15] and classic communication [20]. However, the maximum multiplexing capacity is ultimately restricted by the limited space-bandwidth product (SBP) of the system, which is also a widely discussed issue in the OAM multiplexing communication field [21]. Adequately exploiting the SBP resource is of great importance for capacity expansion.

In OAM holography, the vortex phase of OAM mode is inherited throughout the spatial-frequency transformation by discrete sampling method, endowing the hologram diffraction with OAM preservation and selectivity [13]. The generation method of OAM hologram is similar to the Dammann grating, which is widely used in the field of holographic imaging and OAM

#430882 https://doi.org/10.1364/OE.430882
Journal © 2021 Received 19 May 2021; revised 11 Jul 2021; accepted 30 Jul 2021; published 19 Aug 2021

multiplexed communication [22–24]. In optical OAM advancement, the radial dimension has been widely noticed and applied to modify the OAM beams, such as OAM encoding systems [25], increasing OAM transformation efficiency [26,27], and shaping perfect OAM [28]. However, the radial dimension has not been exploited for enhancing system capacity yet, especially in the holography context. We find that the radial axicon phase modulation also characterizes the similar holographic preservation and selectivity properties like the vortex phase. The combination of the axicon and vortex modulation generates perfect OAM modes [29]. The perfect OAM holography enjoys an excess degree of freedom than conventional OAM holography that might benefit the expanding of information capacity and suppressing channel crosstalk.

Here, we firstly demonstrate the two-dimensional (2D) spatial division multiplexed (SDM) holography with perfect OAM modes. The principle of 2D (radial-angular) perfect OAM multiplexing is verified, including the holography preservation, selectivity and the independence between the radial and angular channels. The axicon coefficient can continuously control the crosstalk between mode channels. This means the inter-channel TC step is extricated from the requirement of channel fidelity. As a result, we increase the OAM channel resolution of the holography from integer-order to 0.01, which is the finest fractional TC detection resolution in the latest reports [30,31]. The scheme of ultra-fine OAM-dependent holography is illustrated with seven fractional OAM modes ranges from l=0 to l=0.06. To fully utilize the perfect OAM channel resource, the 2D (spatial-domain axicon and vortex) modulations should be multiplexed. A 2D SDM holography is designed and further applied to an encryption demonstration, with 20-digit patterns encrypted and multiplexed in a limited SBP less than 20. The perfect OAM modes can provide high capacity, security and SBP efficiency to the holography multiplexing.

2. Results

2.1. Principle of perfect OAM holography

The working mechanism of axicon and vortex phase modulation in terms of perfect OAM generation is illustrated in Fig. 1(a), including beam profiles in the frequency domain and their normalized intensity distribution (along the white lines). Both axicon and vortex phase modulations on a Gaussian beam generate ring-shape beams. The central intensity of the vortex-phase generating OAM pattern is strictly zero due to the phase singularity. Meanwhile, the axicon phase modulation provides a radius-controllable ring-shape spot. It is worth noting that the sampling spot radius is determined by the continuously axicon coefficient, which could also negatively value. The combination of the axicon and vortex modulation is the phase mask that generates perfect OAM modes in the frequency domain. Figure 1(b) is the schematic illustrating the diffraction effect of the discrete sampling hologram to a ring-shape beam profile. The hologram duplicates and shifts the incident beam in the frequency domain by adding extra lateral spatial frequency. The space between sampling spots saves the ring-shape beams from mutual interference and provides the ring-shape preservation to the holography. The simulated results illustrating the radial and OAM (angular) preservation are present in Fig. 1(c1) and 1(c2), respectively. The CGH is designed to construct the discrete sample pattern of letter ‘H’ in the frequency domain. Superposing the axicon-vortex modulation and the discrete sampling hologram constructs a perfect OAM selective hologram (Fig. 1(d)). The hologram is then inserted to a spatial-frequency transformation optical path for image reconstruction. Filtered by a discrete sampling aperture array, the information of pattern ‘H’ is hidden unless the incident beam is appended with two preset decoding keys, the corresponding axicon coefficient -p_1 and vortex TC l=-2.

The radial-multiplexed holography experiment has been implemented (Fig. 2) to verify the feasibility of the axicon modulation. The radial preservation is examined by a monolithic hologram constructing the beam pattern ‘SZU’, the abbreviation of ‘*Shenzhen University*’. The

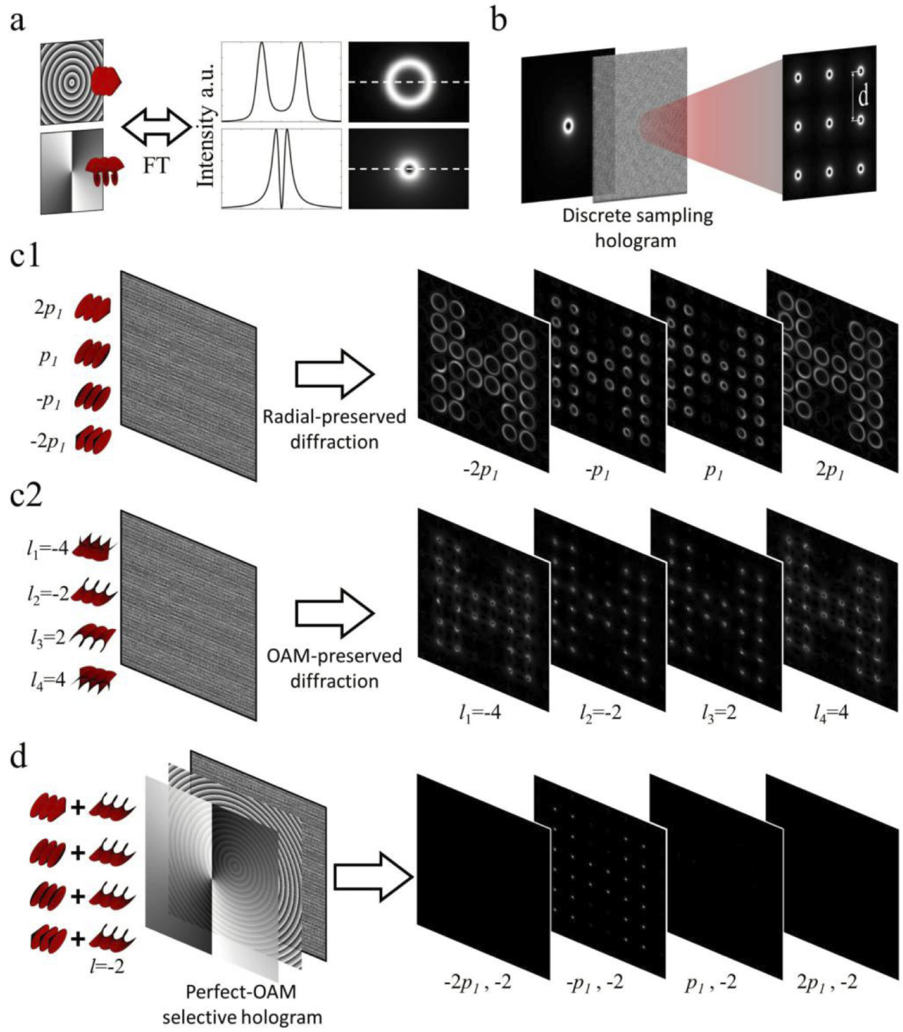

Fig. 1. Principle of perfect OAM holography. **a**, working mechanism of axicon and vortex modulation through the spatial and frequency domain. Left: the phase distribution of spatial domain axicon and vortex modulation. Right: the intensity distribution and the profile of the frequency domain modulated beam. **b**, The schematic of discrete sampling hologram to a ring-shape beam. **c1**, The radial preserved diffraction and **c2**, the OAM preserved diffraction of a discrete sampling hologram to various axicon and vortex modified incident beams. **d**, Image deciphering of a perfect OAM selective hologram.

simulation target and the experiment pattern are presented in Fig. 2(a). With various axicon-modulated incident beams, the radial holography preservation is presented (Fig. 2(c1)) despite interference existing at the boundary. It is induced by the insufficient discrete sampling space interval. The bright beam spot at the bottom is the zero-order diffraction, which presents the undisturbed diffraction pattern of the incident beam. In the radial preservation demonstration, the radial coefficient difference between the illustrated three incident beams is 4.8 mm^{-1}, and the beam profile at each sampling spot is the same as the zero-order spot. The radial selective hologram is superposed by three individual holograms, which is appended with corresponding axicon-modulated phases (Fig. 2(b)). For the convenience of the channel crosstalk analysis, the

Optics EXPRESS

three letters are designed at different positions. The radial-multiplexing results are demonstrated in Fig. 2(c2), where the hologram ‘S’ is attached with axicon coefficient -4.8 mm^{-1}, ‘Z’ without radial modulation and ‘U’ with axicon coefficient 4.8 mm^{-1}. Therefore, only an incident beam with the corresponding compensating axicon coefficient could convert the target letter into Gaussian-like points while the other letters remain in ring-shape. Filtered by an aperture array, only the target reconstructing pattern can be retained. It should be mention that the applied axicon coefficient is limited by the discrete sampling space interval. Although a larger axicon coefficient seems to enlarge the ring radius and eliminate the undesired letters, unrestricted increasing could raise interference between sampling points and crosstalk between multiplexing channels.

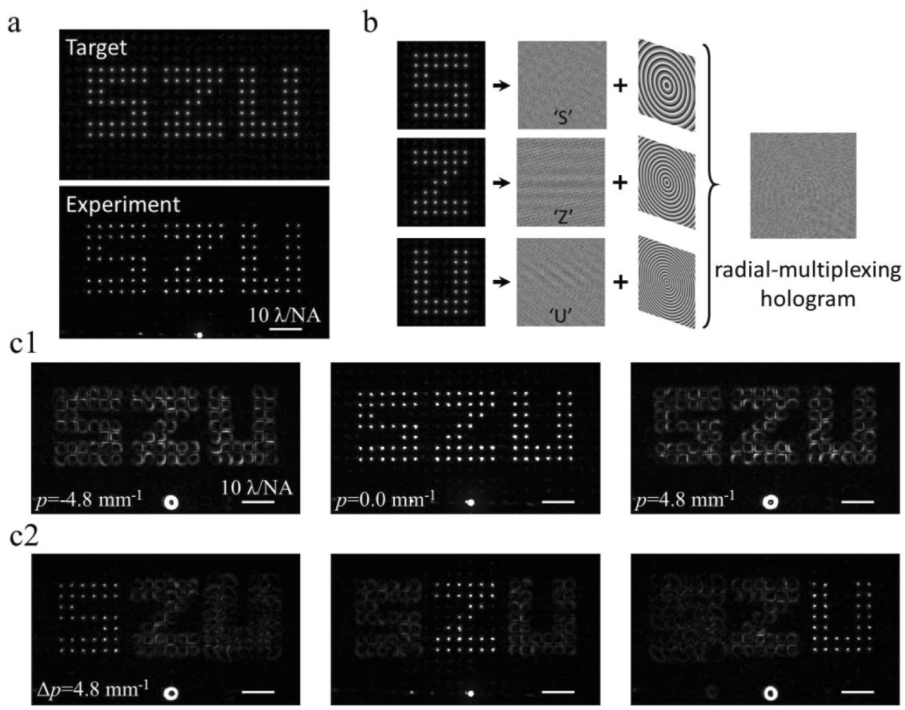

Fig. 2. Experiment inspection of the radial multiplexed holography. a, The target and experiment beam pattern reconstructed by a monolithic hologram. **b**, the generation method of a hybrid radial multiplexing hologram. **c1**, Experiment verification of radial preservation diffraction based on the monolithic hologram (shown in a). **c2**, The axicon phase decoding of the hybrid radial-multiplexing hologram (shown in b).

2.2. Ultra-fine OAM multiplexing holography

In virtual of the independence between the radial and angular phase modulation, the conventional OAM holography can be further divided by the axicon phase modulation. Therefore, the 1D SDM ultra-fine OAM holography is proposed and implemented (Fig. 3(a)), where the discrimination between the perfect OAM modes is mainly according to the axicon modulation and the TCs only play the role of channel characterization. As a result, the TC step between adjacent OAM channels can be intensely compressed. The super-fine OAM holography with 0.01 TC resolution is achieved in Fig. 3(b) and 3(c). Compared to the result shown in Fig. 2, the number of displaying letters is extended to seven, where ‘COFS’ is the abbreviation of ‘*Centre of Fiber Sensors*’. In order to display seven letters within our limited CCD working area, the discrete sampling space interval is half to that in Fig. 2(a). The smaller sampling space interval leads to the

Optics EXPRESS

degradation of beam pattern quality. Figure 3(c1) to (c7) exhibit the decoding results of the ultra-fine OAM-dependent holography, where the TC values from 0 to 0.06 with the step of 0.01, and the axicon coefficients range from -12 mm^{-1} to 12 mm^{-1} with the step of 4 mm^{-1} accordingly. As the maximum axicon coefficient difference setting 24 mm^{-1}, the radius of the ring-shape spot is larger than the sampling space interval between adjacent points. Therefore, the radial preservation holography of the unselected letters is wholly destroyed, and the pattern is blurry. On the contrary, the selected letter pattern can be displayed clearly. A logical point array mask with point radius of 3 pixels is added to the recorded images to filter the blurry part. Ultimately, the ultra-fine OAM-dependent holography is implemented with dense discrete sampling points.

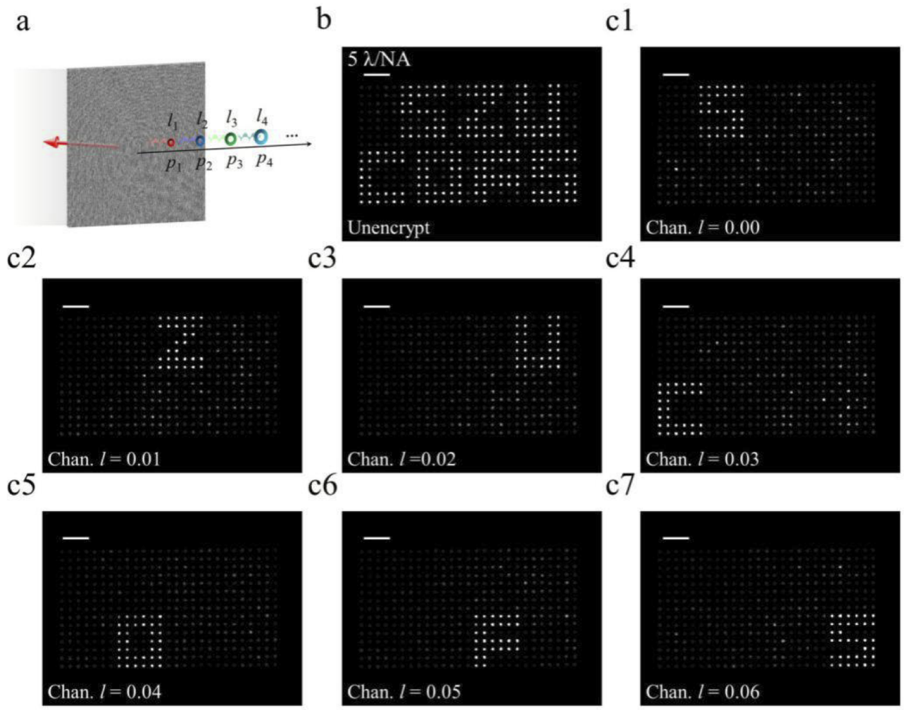

Fig. 3. **Ultra-fine OAM multiplexing holography.** **a**, Concept of one-dimension spatial division multiplexed holography with perfect OAM modes. **b**, Reconstructed seven-letter pattern with dense discrete sampling points. **c1-c7**, Demonstration of ultra-fine fractional OAM multiplexing holography, where the incident beams are modulated with corresponding vortex TCs (from 0 to 0.06) and axicon coefficients (from -12 mm^{-1} to 12 mm^{-1}).

2.3. 2D SDM holography and high-security encryption

Similar to the conventional OAM holography, the ultra-fine OAM-dependent holograp hy is also constructed under the frame of 1D SDM. Although the OAM TC exploiting density has been increased, the actual multiplexing capacity has not been boosted yet. Making full use of the radial and angular phase modulation can achieve the 2D SDM holography (Fig. 4(a)), where the composition of radial and angular phase modulation constructs perfect OAM mode and the holography capacity is enhanced. Simultaneously, the security of the holography could also be improved with the extension of multiplexing channel numbers, as the axicon coefficient value continues and infinite. The construction of high-security 2D SDM hologram is shown in Fig. 4(b). In order to maintain the perfect OAM preservation, a two-time larger discrete sampling space interval is adopted than that in Fig. 3. The axicon and vortex phase that superposed as the perfect OAM modulation are loaded to the corresponding individual hologram (Fig. 4(b)). The multiplexing result is exhibited in Fig. 4(c1) to (c3). Due to the channel division, the three letters are not focused simultaneously in the frequency domain. A discrete aperture array is applied to filter the undesired ring-shape spots during the de-multiplexing. In the 2D SDM holography, the TC step should take large enough. Otherwise, the high crosstalk arises as shown in Fig. 3(c1). The channel crosstalk between TC 0, 1 and 2 is only around -2 dB so that the letter patterns are mixed. The crosstalk is calculated by the logarithm of the ratio of target and undesired pattern intensity. In Fig. 4(c2), the axicon coefficient difference 3.2 mm^{-1} provides the low crosstalk of around -8 dB. By superposing the axicon and vortex phase together, the crosstalk is suppressed to around -10 dB (Fig. 4(c3)), which increase the display quality of the 3-letter multiplexing hologram. In order to achieve more multiplexing channels and exhibit the characteristic of high capacity, it is necessary to increase the axicon coefficient and vortex TC difference to reduce crosstalk.

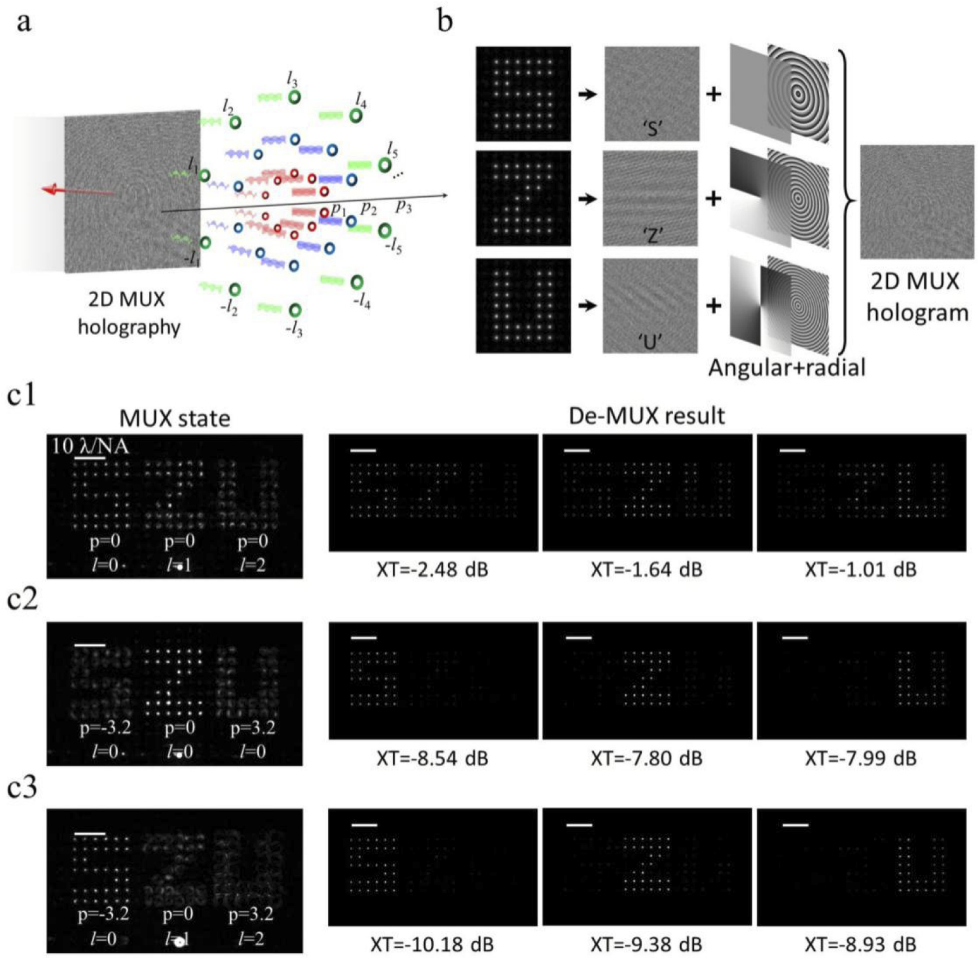

Fig. 4. Two-dimension spatial division multiplexed holography. a, Schematics of large capacity perfect OAM holography. **b,** Superposition approach of the high capacity hologram. **c,** The multiplexing state and de-multiplexing result of holograms with, **c1,** vortex TC step of 1, **c2,** axicon coefficient step of 3.2 mm^{-1}, and **c3,** combination of vortex and axicon modulation.

Optics EXPRESS

The 20-digit high-security holography encryption is designed and demonstrated using 20 perfect OAM modes (Fig. 5), including four axicon coefficients, from -4.8 mm^{-1} to 4.8 mm^{-1}, and five OAM TCs from -16 to 16. For high multiplexing fidelity, the sampling space interval is extended to around 10λ/NA, and the pattern is almost full of our camera screen (10.24 mm×12.80 mm). This predicament of insufficient camera size can be optimized with proper incident beam size, wavelength and focus length. The reconstructed Arabic numbers are listed in Fig. 5(b), and each is decoded by single perfect OAM mode with two decoding keys. Furthermore, a total of 100 tens digits can be displayed with superposition mode incidence. Three examples are presented in Fig. 5(c) with corresponding two-mode mixed states, and each possesses four decoding keys that ensure high security. We chose the decimal Arabic numbers for demonstration. The information entropy of each figure is $\log_2(20)$ bits with single state incident and $\log_2(100)$ bits with superposition state incident. However, it worth noting that the maximum usage of 20

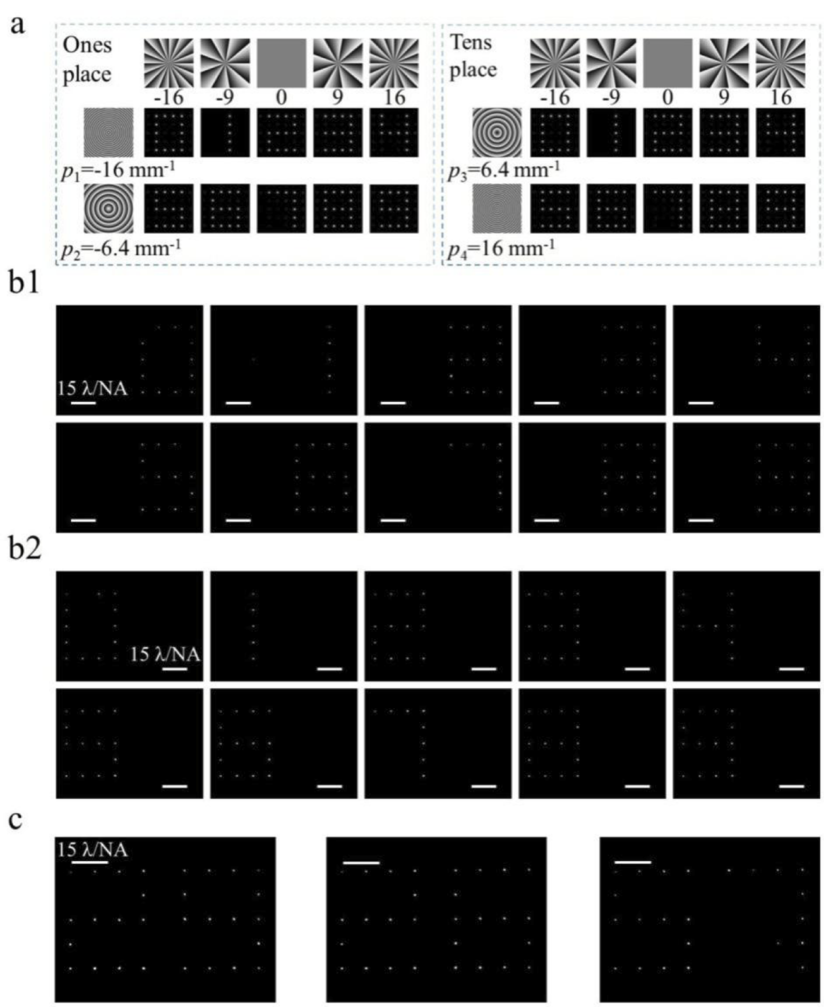

Fig. 5. The 20-digit multiplexed perfect OAM holography encryption. a, Mode states exploited and their corresponding relationship in the multiplexed holography demonstration. The exhibition of ten Arabic numbers set on **b1,** ones place, **b2,** tens place. **c,** three of 100 tens digits decoded by the superposed perfect OAM incident beam.

Optics EXPRESS

multiplexing states is in binary (2^{20} digits) and the maximum information entropy of a single pattern is 20 bits.

3. Discussion

We have improved the conventional OAM holography by adding the radial modulation as a new degree of freedom and proposed perfect SDM OAM holography. On the one hand, the radial modulation can independently suppress the crosstalk between multiplexing channels, as such contributing to the construction of ultra-fine OAM-dependent holography multiplexing. Based on this principle, a 0.01 TC resolution seven-mode fractional OAM holography is then demonstrated. Due to the crosstalk induced by insufficient discrete sampling space interval, the reconstructed patterns are separated and displayed at different positions. However, limited by our camera size (10.24 mm×12.80 mm), only seven patterns are exhibited in our experiment. The multiplexing channel can be further elevated with a larger displaying area. On the other hand, the massive multiplexing channel resource provided by radial modulation is compatible with conventional multiplexing approaches and conductive to the holography capacity enhancement. The 2D SDM holography is constructed by adding the radial modulation to the conventional OAM holography. A 3.2 mm^{-1} axicon coefficient brings about -8 dB crosstalk suppression in our demonstration system. Furthermore, in holography encryption, the radial modulation (axicon coefficient) also provides security as an additional decryption key. We demonstrated a 20-mode perfect OAM holography encryption. In virtual of the high-capacity of 2D SDM, the SBP utilizing efficient is elevated one order of magnitude than the latest conventional phase-only OAM holography [13]. We also constructed 100-digit holography by the concept of two-OAM-mode superposed decryption, where the decoding key amount is doubled. To summarize, the perfect OAM holography exhibits great potential in related applications such as information storage, image encryption and holographic optical switching, optical tweezing and optical computing.

Funding. Science and Technology Innovation Commission of Shenzhen (JCYJ20180507182035270, JCYJ20180507182058432); Natural Science Foundation of Guangdong Province (2019A050510047, 2019B1515120042); China Postdoctoral Science Foundation (2021M692176); National Natural Science Foundation of China (61635007, 61875134, 62005169).

Disclosures. The authors declare no conflicts of interest.

Data availability. The supporting data of this work is available from the corresponding authors upon reasonable request.

References

1. X. Lin, Y. Rivenson, N. T. Yardimci, M. Veli, Y. Luo, M. Jarrahi, and A. Ozcan, "All-optical machine learning using diffractive deep neural networks," Science **361**(6406), 1004–1008 (2018).
2. Y. Rivenson, Y. Wu, and A. Ozcan, "Deep learning in holography and coherent imaging," Light. Sci. Appl. **8**(1), 85 (2019).
3. M. Padgett and R. Di Leonardo, "Holographic optical tweezers and their relevance to lab on chip devices," Lab on a Chip. **11**(7), 1196–1205 (2011).
4. K. Dholakia and T. Čižmár, "Shaping the future of manipulation," Nat. Photonics **5**(6), 335–342 (2011).
5. K. T. Lim, H. Liu, Y. Liu, and J. K. Yang, "Holographic colour prints for enhanced optical security by combined phase and amplitude control," Nat. Commun. **10**, 25 (2019).
6. G. Wetzstein, A. Ozcan, S. Gigan, S. Fan, D. Englund, M. Soljačić, C. Denz, D. A. Miller, and D. Psaltis, "Inference in artificial intelligence with deep optics and photonics," Nature **588**(7836), 39–47 (2020).
7. J. F. Heanue, M. C. Bashaw, and L. Hesselink, "Volume holographic storage and retrieval of digital data," Science **265**(5173), 749–752 (1994).
8. X. Li, L. Chen, Y. Li, X. Zhang, M. Pu, Z. Zhao, X. Ma, Y. Wang, M. Hong, and X. Luo, "Multicolor 3D meta-holography by broadband plasmonic modulation," Sci. Adv. **2**(11), e1601102 (2016).
9. S. Chang, X. Guo, and X. Ni, "Optical metasurfaces: progress and applications," Annu. Rev. Mater. Sci. **48**(1), 279–302 (2018).
10. D. Wen, F. Yue, G. Li, G. Zheng, K. Chan, S. Chen, M. Chen, K. F. Li, P. W. H. Wong, K. W. Cheah, and E. Y. B. Pun, "Helicity multiplexed broadband metasurface holograms," Nat. Commun. **6**(1), 1–7 (2015).

Optics EXPRESS

11. S. M. Kamali, E. Arbabi, A. Arbabi, Y. Horie, M. Faraji-Dana, and A. Faraon, "Angle-multiplexed metasurfaces: encoding independent wavefronts in a single metasurface under different illumination angles," Phys. Rev. X **7**(4), 041056 (2017).
12. H. Ren, G. Briere, X. Fang, P. Ni, R. Sawant, S. Héron, S. Chenot, S. Vézian, B. Damilano, V. Brändli, and S. A. Maier, "Metasurface orbital angular momentum holography," Nat. Commun. **10**, 2986 (2019).
13. X. Fang, H. Ren, and M. Gu, "Orbital angular momentum holography for high-security encryption," Nat. Photonics **14**(2), 102–108 (2020).
14. N. Bozinovic, Y. Yue, Y. Ren, M. Tur, P. Kristensen, H. Huang, A. E. willner, and S. Ramachandran, "Terabit-scale orbital angular momentum mode division multiplexing in fibers," Science **340**(6140), 1545–1548 (2013).
15. G. Vallone, V. D'Ambrosio, A. Sponselli, S. Slussarenko, L. Marrucci, F. Sciarrino, and P. Villoresi, "Free-space quantum key distribution by rotation-invariant twisted photons," Phys. Rev. Lett. **113**(6), 060503 (2014).
16. J. Wang, J. Yang, I. M. Fazal, N. Ahmed, Y. Yan, H. Huang, Y. Ren, Y. Yue, S. Dolinar, M. Tur, and A. E. Willner, "Terabit free-space data transmission employing orbital angular momentum multiplexing," Nat. Photonics **6**(7), 488–496 (2012).
17. H. Ren, X. Fang, J. Jang, J. Bürger, J. Rho, and S. A. Maier, "Complex amplitude metasurface-based orbital angular momentum holography in momentum space," Nat. Nanotech. **15**(11), 948–955 (2020).
18. R. Zhao, B. Sain, Q. Wei, C. Tang, X. Li, T. Weiss, L. Huang, Y. Wang, and T. Zentgraf, "Multichannel vectorial holographic display and encryption," Light Sci. Appl. **7**(1), 1–9 (2018).
19. Z. Zhou, Y. Hua, X. Liu, G. Chen, J. Xu, Y. Han, C. Li, and G. Guo, "Quantum Storage of Three-Dimensional Orbital-Angular-Momentum Entanglement in a Crystal," Phys. Rev. Lett. **115**(7), 070502 (2015).
20. G. Gibson, J. Courtial, M. J. Padgett, M. Vasnetsov, V. Pas'ko, S. M. Barnett, and S. Franke-Arnold, "Free-space information transfer using light beams carrying orbital angular momentum," Opt. Express **12**(22), 5448–5456 (2004).
21. N. Zhao, X. Li, G. Li, and J. M. Kahn, "Capacity limits of spatially multiplexed free-space communication," Nat. Photonics **9**(12), 822–826 (2015).
22. P. García-Martínez, M. M. Sánchez-López, J. A. Davis, D. M. Cottrell, D. Sand, and I. Moreno, "Generation of Bessel beam arrays through Dammann gratings," Appl. Optics **51**(9), 1375–1381 (2012).
23. T. Lei, M. Zhang, Y. Li, P. Jia, G. N. Liu, X. Xu, Z. Li, C. Min, J. Lin, C. Yu, and H. Niu, "Massive individual orbital angular momentum channels for multiplexing enabled by Dammann gratings," Light Sci. Appl. **4**(3), e257 (2015).
24. N. Zhang, X. Yuan, and R. Burge, "Extending the detection range of optical vortices by Dammann vortex gratings," Opt. Lett. **35**(20), 3495–3497 (2010).
25. Z. Guo, Z. Wang, M. I. Dedo, and K. Guo, "The orbital angular momentum encoding system with radial indices of Laguerre–Gaussian beam," IEEE Photonics J. **10**(5), 1–11 (2018).
26. Y. Wen, I. Chremmos, Y. Chen, J. Zhu, Y. Zhang, and S. Yu, "Spiral transformation for high-resolution and efficient sorting of optical vortex modes," Phys. Rev. Lett. **120**(19), 193904 (2018).
27. S. Li and J. Wang, "A compact trench-assisted multi orbital angular momentum multi-ring fiber for ultrahigh-density space-division multiplexing (19 rings× 22 modes)," Sci. Rep. **4**(1), 3853 (2015).
28. M. Pu, X. Li, X. Ma, Y. Wang, Z. Zhao, C. Wang, C. Hu, P. Gao, C. Huang, H. Ren, and X. Li, "Catenary optics for achromatic generation of perfect optical angular momentum," Sci. Adv. **1**(9), e1500396 (2015).
29. P. Vaity and L. Rusch, "Perfect vortex beam: Fourier transformation of a Bessel beam," Opt. Lett. **40**(4), 597–600 (2015).
30. Z. Liu, S. Yan, H. Liu, and X. Chen, "Superhigh-Resolution Recognition of Optical Vortex Modes Assisted by a Deep-Learning Method," Phys. Rev. Lett. **123**(18), 3902 (2019).
31. G. Zhu, Z. Liu, C. Fu, S. Liu, Z. Bai, and Y. Wang, "High-Precise Fractional Orbital Angular Momentum Probing with a Fiber Grating Tip," J. Lightwave. Technol. **39**(6), 1867–1872 (2021).